Indian J Phys (August 2019) 93(8):1009–1018
https://doi.org/10.1007/s12648-018-01369-4

ORIGINAL PAPER

Investigating of structural, morphology, optical, transport and magnetic properties of $Mg_{1-x}Cu_xO$

S A Gad[2]*, G M El Komy[1], A M Moustafa[2] and A A Ward[3]

[1]Physics Division, Electron Microscope and Thin Films Department, National Research Centre, 33 El Bohouth St. (Former El Tahrir St.), Dokki, P.O. Box 12622, Giza, Egypt

[2]Physics Division, Solid State Physics Department, National Research Centre, 33 El Bohouth St. (Former El Tahrir St.), Dokki, P.O. Box 12622, Giza, Egypt

[3]Physics Division, Microwave Physics and Dielectrics Department, National Research Centre, 33 El Bohouth St. (Former El Tahrir St.), Dokki, P.O. Box 12622, Giza, Egypt

Received: 04 April 2018 / Accepted: 05 October 2018 / Published online: 8 January 2019

Abstract: Effect of Cu^{2+} content on different properties was investigated. $Mg_{1-x}Cu_xO$ ($0.05 \leq x \leq 0.2$) powder was prepared via solid-state reaction. The samples were examined by X-ray diffraction, and the results were analyzed by using Full Prof program by employing Rietveld refinement technique. The results showed that samples with Cu content up to $x = 0.15$ had a single phase of MgO rock salt structure type and for $x = 0.2$ two phases were detected, namely MgO rock salt structure and Cu_2O cuprite cubic phase. Also, it was found a small increase in the lattice constants with increasing the Cu content. Moreover, the crystallite size was found to decrease with increasing the Cu concentration. The morphology was studied by transmission electron microscopy. The optical energy gap was calculated, and it was found that it has two values. The energy gaps decreased with increasing the Cu content. The dielectric constant ε', the loss factor tan δ and conductivity increased with increasing Cu concentration. This increase can be directly related to the increase in the concentration of charge carriers and interfacial polarization effects. The saturation magnetization and the retentivity were found to decrease with the increase in Cu concentrations, but the coercivity increased with increasing Cu content.

Keywords: Crystal structure; Optical properties; Dielectric properties; Magnetic properties

PACS Nos.: 61.50.−f; 78.20.−e; 77.22.−d; 75.50.Pp

1. Introduction

Magnesium oxide (MgO) is one of many advanced engineering materials that have been investigated intensively in recent years because of their potentials for many applications in bulk, powder and thin film forms. Magnesium oxide is a semiconductor/insulator which crystallizes in rock salt/sodium chloride (NaCl)-type cubic structure. It is a nonmagnetic insulator with a band gap of 7.809 eV [1]. Many binary oxides, such as CaO, SrO, BaO, NiO and CoO, like MgO crystallize in rock salt structure [1]. MgO is an attractive material which has many applications [2–15], such as water purification, optoelectronics, microelectronics, and additive in heavy fuel oil, paint, gas separation, bactericides, and insulator in industrial cables, crucibles, and refractory materials superconductor physics, fire retardant, UV protection, dental cement. Moreover, it has been used as an oxide barrier in spin-tunneling devices as well as substrate in superconducting and ferroelectric films. Also, MgO is used in medical and pharmaceutical products [16–18] and toxic waste remediation [19, 20]. On the other hand, recent attention has been focused [21, 22] about the transparency behavior of bulk polycrystalline MgO for infrared electromagnetic waves, the material that can be a potential substitute for sapphire IR-windows and protectors for sensor devices.

MgO nano-powders are very interesting because of their applications in many industrial areas, such as a candidate material for translucent ceramics [23], catalyst, catalyst carriers and absorbent for many pollutants [24]. On the

*Corresponding author, E-mail: samiagad2000@yahoo.com

other hand, Ni/MgO catalysts are prepared by impregnation, precipitation and mechanical mixing methods [25, 26]. Also, MgO nanoparticles have high catalytic activity due to the presence of active sites or oxygen vacancies on surfaces and edges which have the potentiality of charge transfer between substrate and adsorbate [27, 28]. Moreover, Nano-MgO materials are found to catalyze efficiently in a variety of organic reactions due to their high specific area [29, 30]. The applications of MgO can be outspread by adjusting the lattice constant, physical and chemical properties by doping other elements such as Zn, Ni, and Cu. MgO doped with Cu nano-powders was prepared by different methods such as chemical co-precipitation, and the effect of Cu on the morphology and structure was studied [31]. MgO was portending to display magnetic properties, offering possibility applications of Cu-doped MgO as diluted magnetic semiconductors [32]. Thus, the new properties are expected in the MgO doped with other elements. The aim of this work is to study the effect of Cu on the structure, optical, magnetic and dielectric properties of MgO.

2. Sample preparation

Polycrystalline $Mg_{1-x}Cu_x$ O (where x = 0.05, 0.1, 0.15 and 0.2) samples were prepared using solid reaction technique, using high-purity (99.99%) MgO and CuO obtained from Sigma-Aldrich. Stoichiometric amounts of the starting materials were mixed followed by grinding, to get a homogenous mixture. The mixed samples were then compressed under a pressure of 3 ton cm^{-2} in rectangular form. The pressed samples were sintered at 900 °C in air for 23 h. Then, the samples are sintered at 1050 °C for 23 h. Finally, the temperature of the furnace was gradually cooled to room temperature.

3. Experimental details

The X-ray powder diffraction data of the constituent phases were collected on Emprean PANalytical X-ray diffractometer equipped with CuK_α radiation (1.5406 Å) using a step-scanning mode, in the angular range 30–100° 2θ was carried out in the step size 0.02° of 2θ and step time 20 s/step. Diffuse reflection measurements were done in the wavelength range from 200 to 2500 nm using Jasco (V-570) spectrophotometer. A vibrating sample magnetometer model 9600-1-VSM was used for the magnetic properties measurements. In the present study, dielectric and conductivity measurements were carried out by means of high-resolution broadband impedance analyzer (Schlumberger Solartron 1260). The frequency range of the applied ac electric field was between 0. 1 Hz and 1 MHz. Electromagnetic shielding was implemented to the whole sample holder in order to diminish noise problems that are common especially at low frequencies. The measurements were automated by interfacing the impedance analyzer with a personal computer through a GPIB cable IEE488. A commercial interfacing and automation software LabVIEW was used for acquisition of data. The error in ε' and ε'' amounts to 1% and 3%, respectively.

4. Results and discussion

4.1. Structure

The X-ray diffraction patterns for the series $Mg_{1-x}Cu_xO$, $0.05 \leq x \leq 0.2$ are depicted in Fig. 1. Applying the search-match program, X'Pert High Score Plus, for phase analysis, it was found that samples with Cu content up to x = 0.15 resemble a single-phase solid solution of MgO rock salt structure type ICDD Card No. 98-006-0497, of space group Fm-3 m, while for x = 0.2, two phases were detected, namely MgO rock salt structure ICDD Card No. 98-006-0497 and Cu_2O cuprite cubic-phase Card No. 98-017-3982 related to Pn-3 m space group. This indicated that the limited miscibility of Cu^{2+} ions in the MgO lattice to be around 15%. The phase percentage of the $Mg_{1-x}Cu_xO$ rock salt structure from quantitative phase analysis was 82.8% at the doping level x = 0.2. Moreover, as the Cu substitution content is increasing, there was a continuous shift in 2θ toward a low-angle side, indicating corresponding increase in lattice parameters. Figure 2 shows the shifting of (200) peaks, and this is true with the other peaks as well.

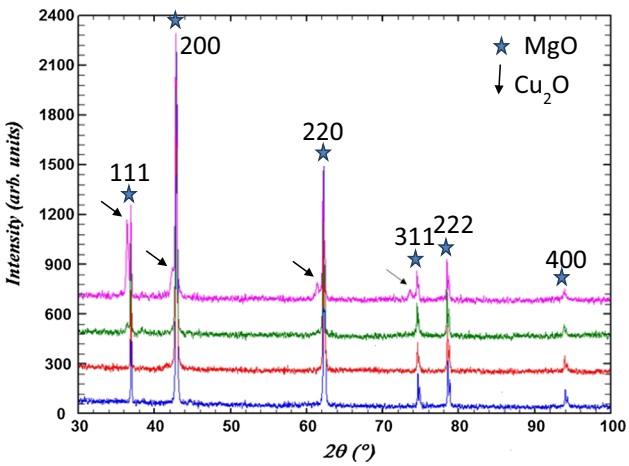

Fig. 1 X-ray powder diffraction pattern for the samples $Mg_{1-x}Cu_xO$, $0.05 \leq x \leq 0.2$

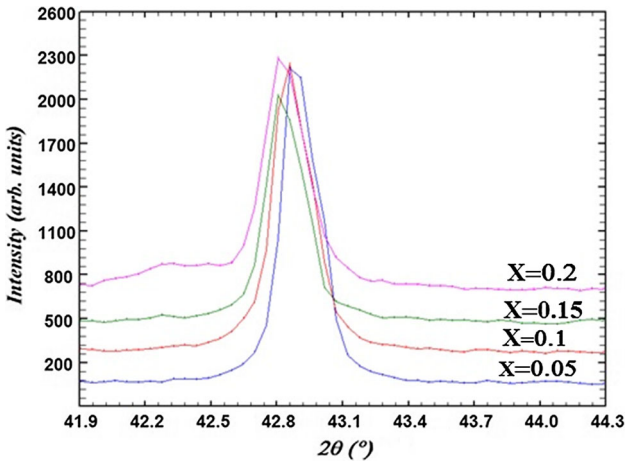

Fig. 2 Zoom on (200) reflection in MgO

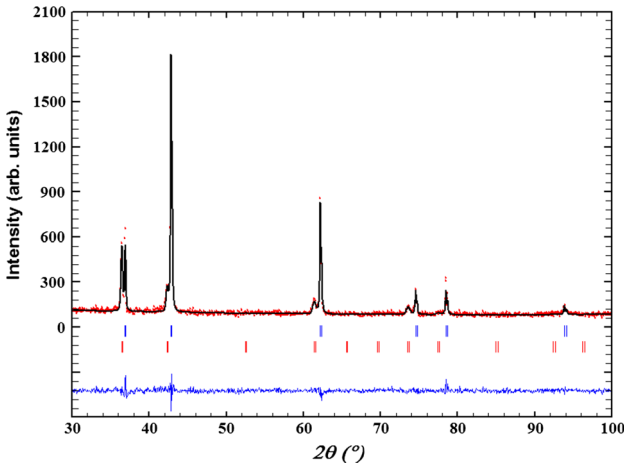

Fig. 3 Final Rietveld refinement for $Mg_{0.95}Cu_{0.05}O$ sample as representative one. The observed (closed circles) and calculated (solid line) X-ray diffraction profiles and the difference between them (on the bottom). Vertical bars refer to calculated Bragg peak positions

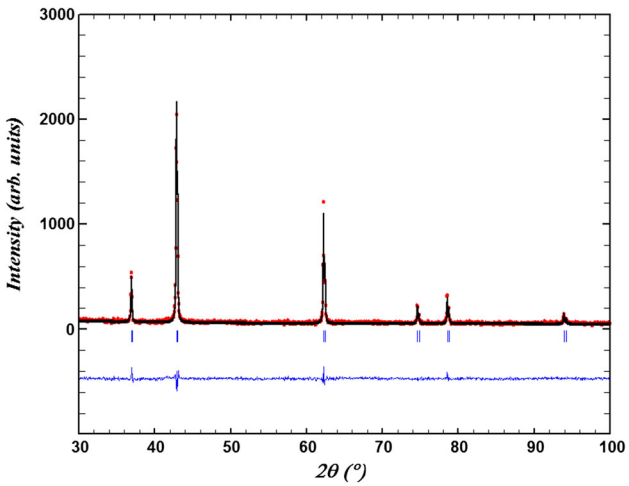

Fig. 4 Final Rietveld refinement for $Mg_{0.8}Cu_{0.2}O$ sample as representative one. The observed (closed circles) and calculated (solid line) X-ray diffraction profiles and the difference between them (on the bottom). Vertical bars refer to calculated Bragg peak positions

In order to extract the structural details from powder diffraction data, all the X-ray diffraction (XRD) patterns were analyzed with the help of Full Prof program by employing Rietveld refinement technique. The method employs a least-squares procedure to compare Bragg intensities and those calculated from a possible structural model. For the samples with doping concentration from 0.05 to 0.15, a single-phase model was used in the refinement, where the space group was Fm-3 m in which the oxygen anions occupy the Wyckoff position 4b, with coordinates 1/2; 1/2; 1/2, while the Mg and Cu cations occupy the A-site at Wyckoff position 4a, with coordinates 0; 0; 0. For the sample with doping level 0.2, a two-phase model was used, one of them was MgO model as before and the other one was for Cu_2O model in which the Cu atom occupies the 4b Wyckoff position 4b, with coordinates 0; 0; 0, and oxygen atom occupies 2a position, with the coordinates 0.25; 0.25; 0.25. A parameterized modified Thompson–Cox–Hasting pseudo-Voigt function [33] was used to fit the peak shape. All the atomic positions were considered as fixed parameters, while other parameters such as lattice constants, isothermal parameters, scale factors and shape parameters were considered as free parameters. The agreement between the observed and calculated diffraction profiles of the sample with $x = 0.05$ and 0.20 as representative examples of the investigated compounds are shown in Figs. 3 and 4. The quality of the agreement between observed and calculated profiles is estimated by profile factor (Rp) and weighted profile factor (Rwp). The small weighted profiles Rp and Rwp illustrate that the proposed model can be reasonable. Table 1 depicts the lattice parameter (a), the unit cell volume, the crystallite size (D) and the XRD density (dx), all obtained from Rietveld refinement. The goodness-of-fit indices are given in Table 1. Their values signify that the fitting qualities are good enough for all experimental patterns.

From the lattice parameter values given in Table 1, it is clearly indicated that there is a small increase in their values from $x = 0.05$ up to $x = 0.15$; this may be due to the difference in the ionic radius between MgO = 0.86 Å and CuO = 0.87 Å. As compared with the lattice parameters of pure MgO, they become nearly constant from $x = 0.15$ up to $x = 0.2$, and this may be due to the effect of the second phase. The crystallite size was found to decrease from 121 to 49 nm with corresponding increase in Cu content from $x = 0.05$ to $x = 0.2$, which means that the Cu acts as the grain growth inhibitor. Also, we can deduce that, with the reduction in particle size associated with lattice expansion, the same behavior was obtained for CeO_2 nano-crystals containing dopants larger than Ce^{4+}, such as Nd^{3+} [34].

Table 1 Refined unit cell parameters and agreement factors of $Mg_{1-x}Cu_xO$ with indicated x

Criteria of fit and structure parameters	x = 0.05	x = 0.10	x = 0.15	x = 0.2
Atomic positions for $Mg_{1-x}Cu_xO$				
Mg	0, 0, 0	0, 0, 0	0, 0, 0	0, 0, 0
Cu	0, 0, 0	0, 0, 0	0, 0, 0	0, 0, 0
O	0.5, 0.5, 0.5	0.5, 0.5, 0.5	0.5, 0.5, 0.5	0.5, 0.5, 0.5
Atomic positions for CuO				
Cu	–	–	–	0, 0, 0
O	–	–	–	0.25, 0.25, 0.25
Isotropic thermal displacement parameter	–	–	–	
O	0.18(4)	1.15(8)	0.11(4)	1.7(2)
Mg	0.19(5)	0.72(5)	0.25(3)	0.81(5)
Cu	0.19(5)	0.72(5)	0.25(3)	0.81(5)
Rp	26.6	31.5	57.0	41.2
Rwp	22.0	23.2	32.3	26.5
Rexp	22.47	24.27	30.88	27.68
a (Å)	4.21297(1)	4.21530(1)	4.21835(2)	4.21844(2)
Cell volume ($Å^3$)	74.776(2)	74.901(1)	75.063(1)	75.068(1)
Crystallite size (nm)	121	60	63	49
Density (gm/cm^3)	3.892	3.922	4.393	4.234
Mg–O	2.1065	2.1076	2.1092	2.1092
O–O	2.9790	2.9807	2.9828	2.9829

The MgO crystal structure can be described as cubic closely packed structure of oxygen atoms and Mg atoms occupying octahedral sites, i.e., each Mg cations surrounded by six oxygen anions as shown in Fig. 5, in which the interatomic distances are Mg–O ranging from 2.1065 to 2.1092 Å and O–O ranging from 2.9790 to 2.9829 Å as the copper doping increases, and this may be due to the difference in the ionic radius between Mg^{2+} and Cu^{2+}.

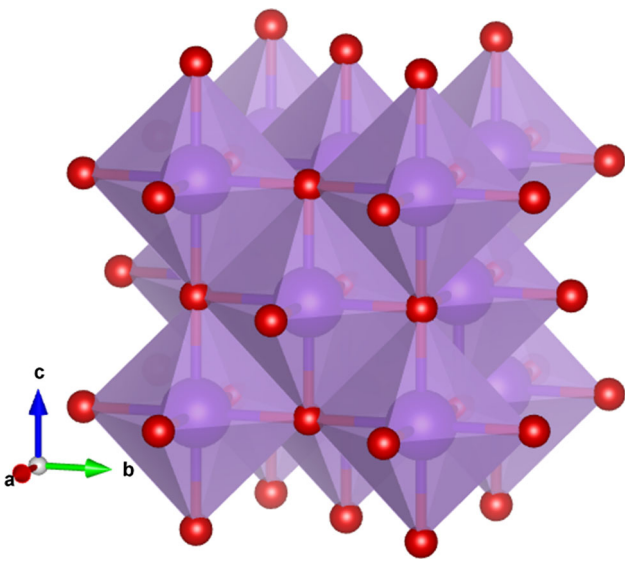

Fig. 5 MgO crystal structure, the Mg cation surrounded by six oxygen anions forming octahedra

4.2. Morphological studies (TEM)

Figure 6a–d shows the HR-TEM images of $Mg_{1-x}Cu_xO$. All images indicate aggregates of uniform shapes of nanoparticles for all samples doped with different Cu concentrations. The described aggregates composed of sets of welded uniform sphere-like particles (see inset Fig. 6a, b). The particles in the aggregates have diameters in the range from 5 to 80 nm as the Cu content increases from x = 0.05 to 0.2 as clearly observed from Fig. 6a–d. Furthermore, more welded and clear boundaries of nanoparticles can be observed with increasing Cu content in MgO. The average particle size detected from the HR-TEM micrographs is smaller than that obtained from XRD measurement due to the difference in the resolution of both analyses. The corresponding selected area electron diffraction (SAED) of all samples shows highly oriented polycrystalline structure with very fine particles in the aggregates. The orientation increases with increasing the Cu content. The information obtained from the electron microscopy investigations is in line with that obtained from the XRD analysis.

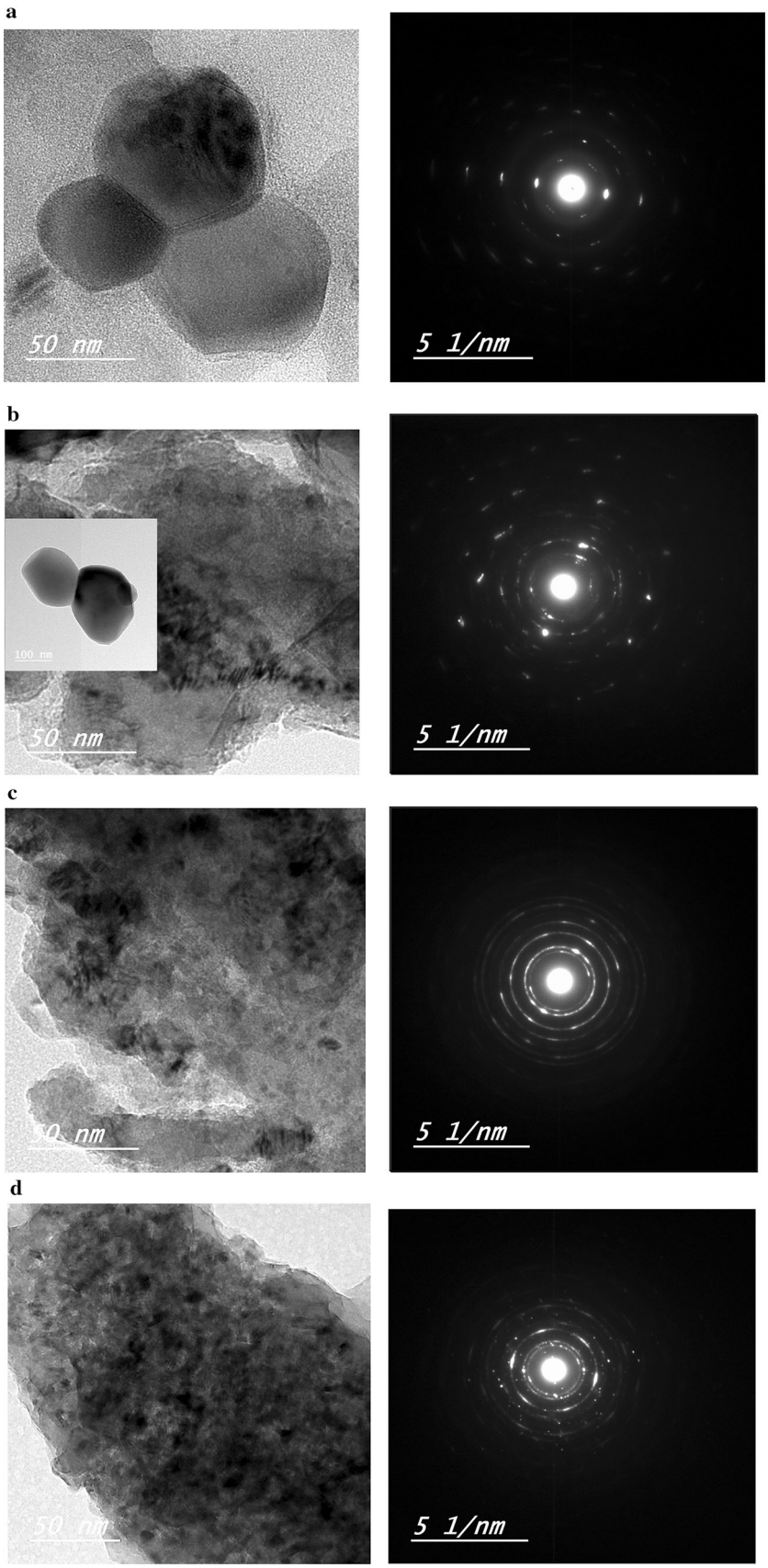

Fig. 6 HRTEM images of $Mg_{1-x}Cu_xO$, where $0.05 \leq x \leq 0.2$ (**a**) $x = 0.05$, (**b**) $x = 0.1$, (**c**) $x = 0.15$ and (**d**) $x = 0.2$

4.3. Optical properties

The diffuse reflectance spectrum of semiconductor powder is analogous to their transition spectrum. A study of the tail of the absorption curve of semiconductor shows that it has an exponential drop [35]. The onset of this drop was taken and suggested as a more universal method of deducing the position of the absorption edge [36]. So, Fosch [36] has taken the onset of the linear increase in diffuse reflectance R, i.e., the linear decrease in the absorption spectrum as a measure of the forbidden gap.

The diffuse reflectance spectra of $Mg_{1-x}Cu_xO$ (x = 0.05, 0.1, 0.15, 0.2) were measured in the spectral range 200–2000 nm. To calculate the optical band-gap energy (E_g), the fundamental absorption of light, which corresponds to an electronic excitation from the valence band to the conduction band, can be applied. Figure 7 shows the reflectance spectra of pure MgO- and Cu-doped samples with different concentration of Cu. Further, the optical band gap is evaluated using K–M function as follows [37]:

$$K/S = (1-R)^2/2R, \quad (1)$$

where R is the absolute reflectance of the sample, K is the molar absorption coefficient, and S is the scattering coefficient. It is shown that from Fig. 7, there are two optical energy gaps, which previously reported that CuO has two optical energy band gaps [38]. A decrease in the energy band gap may be due to the combination of higher band-gap material MgO with smaller band-gap material CuO and may be due to the increase in the lattice constants [39, 40]. Figure 8 shows the relation between energy gaps and the Cu content. The values of the energy gaps are given in Table 2.

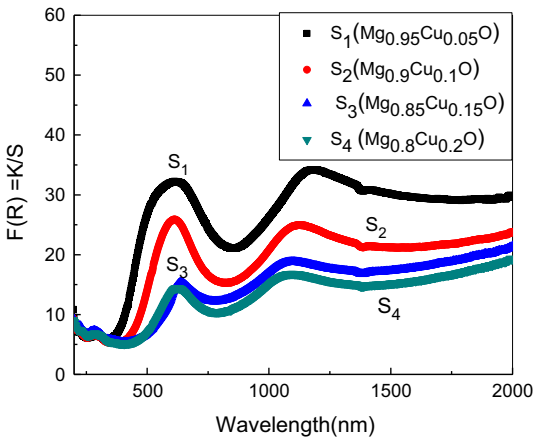

Fig. 7 K/S versus the wavelength λ for $Mg_{1-x}Cu_xO$

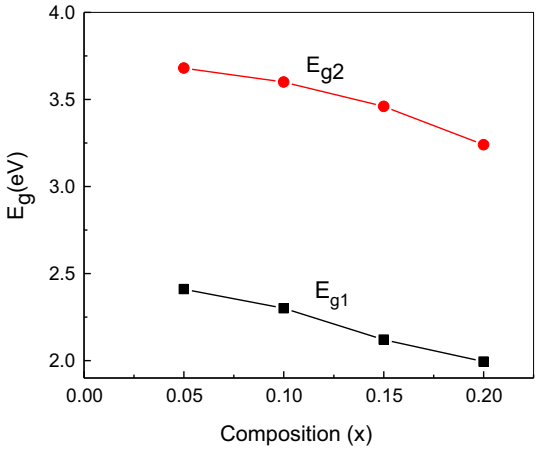

Fig. 8 Optical energy band gap as a function of Cu content

Table 2 Calculated values of the optical energy gaps of $Mg_{1-x}Cu_xO$

Composition (x)	Optical energy gaps	
	(E_{g1})	(E_{g2})
0.05	2.41	3.68
0.1	2.3	3.6
0.15	2.12	3.46
0.2	1.994	3.24

4.4. Dielectric properties

Plots of the dielectric constant (ε') and loss factor (tan δ) versus frequency for the series $Mg_{1-x}Cu_xO$, $0.05 \leq x \leq 0.2$ are illustrated in Figs. 9 and 10 respectively. Obviously, the permittivity (ε') decreases with increasing frequency till reaching a constant value at higher frequencies. The highest values of permittivity at low frequencies are due to interfacial polarization effects associated with an inhomogeneous dielectric medium holding layers of materials with different permittivity and conductivity. Moreover, an increase in ε' by increasing Cu doping can be seen in Fig. 9. This increase can be directly related to the increase in the concentration of (Cu^{2+} ions) dissolved in MgO lattice. Moreover, it can be explained based on the defect change according to Warren et al. [41]. Accordingly, the presence of defect dipoles such as cations of Cu^{2+} formed by Cu doping assists to increase the total polarizability of the medium, which in turn gives rise to the dielectric constant of Cu-doped Mg. Moreover, the presence of Cu^{2+} in MgO lattice may result in more localization of charge carriers in conjunction with mobile ions causing higher ionic conductivity, and this can be another reason for strong low-frequency dispersion of dielectric constant. However, this result is in a good agreement with

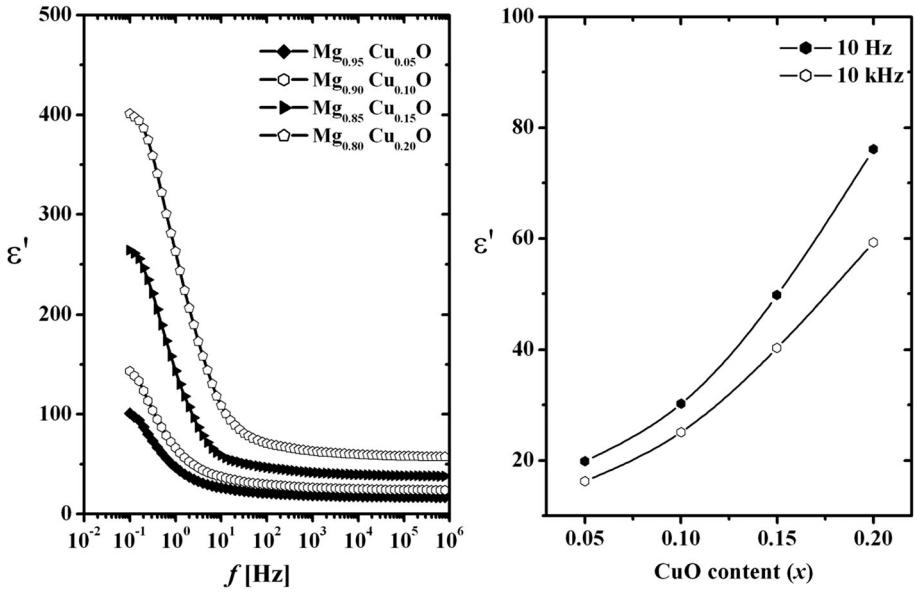

Fig. 9 Dependence of the dielectric constant ε' on frequency for $Mg_{1-x}Cu_xO$, $0.05 \leq x \leq 0.2$ at room temperature (30 °C). The right-side image shows the data of dielectric constant ε' at fixed frequencies of 10 Hz and 10 kHz, respectively

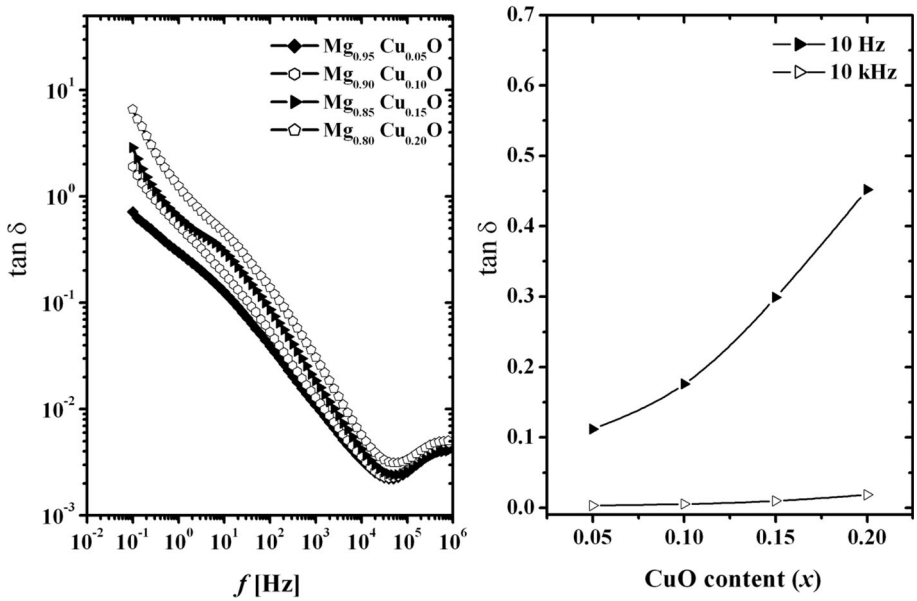

Fig. 10 Dependence of the loss factor tan δ on frequency for $Mg_{1-x}Cu_xO$, $0.05 \leq x \leq 0.2$ at room temperature (30 °C). The right-side image show the data of tan δ at fixed frequencies of 10 Hz and 10 kHz, respectively

the results of XRD measurements, which revealed that the Cu ion substitutes for the Mg ion in the MgO lattice.

On the other hand, Fig. 10 for tan δ shows a broad relaxation process in the low-frequency region for all the investigated samples within the frequency range (0.1 Hz–1 MHz). This relaxation process is attributed to Maxwell–Wangeror interfacial polarization, arising from building up of charges on boundaries and interfaces between materials with different electrical properties [42, 43].

However, it is slightly shifted toward higher frequency range with increasing the Cu doping due to the increase in the conductivity of the samples. Ionic conductance probably results from mobile protons arising from Cu^{2+} ions dissolved in MgO lattice that is reflected by both an increase in free charge mobility and the shift of the peak toward the high-frequency side with a synchronized increase in its magnitude. The overall result is an enhancement of conductivity on addition of Cu.

4.4.1. *Electrical conductivity*

The variation of ac electrical conductivity versus the frequency is depicted in Fig. 11. From this figure, it is obvious that the electrical conductivity σ increases as the frequency increases in accordance with universal power law $\sigma(\omega) = \sigma_{dc} + A\omega^s$, [44, 45].

where A is dependent on temperature, σ_{dc} is the dc conductivity (frequency-independent plateau in the low-

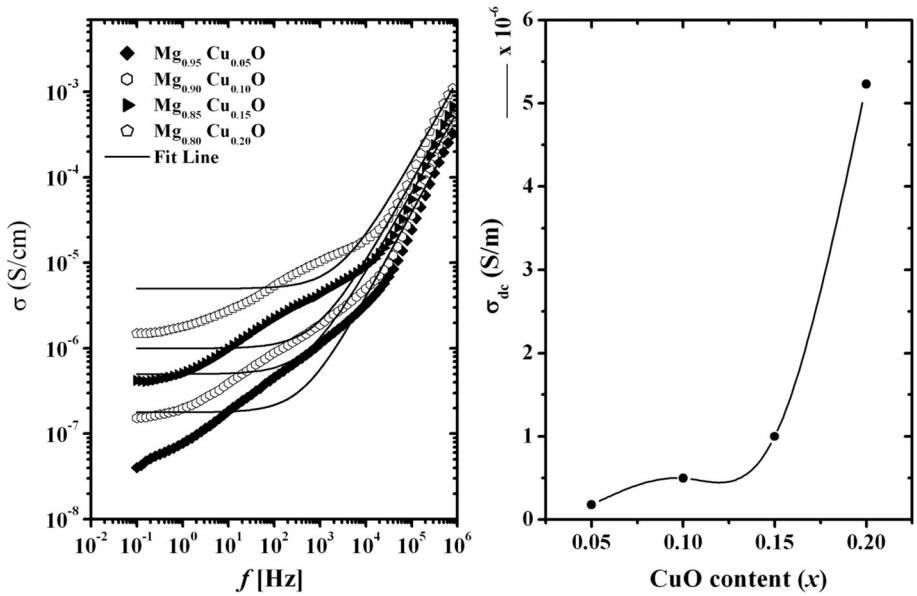

Fig. 11 Dependence of the electrical conductivity σ on frequency for $Mg_{1-x}Cu_xO$, $0.05 \leq x \leq 0.2$ at room temperature (30 °C). The right-side image show the data of dc conductivity for $Mg_{1-x}Cu_xO$, $0.05 \leq x \leq 0.2$ at room temperature (30 °C)

frequency region), the factor s was calculated from the slope of the logarithmic plot between σ and the angular frequency, where $0 < s < 1$. In general, for ionic conductors, the values of exponent s lie between 0.5 and 1 demonstrating ideal long-range drift and limited hopping diffusion (tortuous pathway) [46]. Stand on, the obtained results; s is slightly decreasing by Cu doping ($0.845 < s < 0.955$). These values of exponent-s clarify that the long-range pathway of ions could be one of the sources of the ion conduction. However, the right-side image in Fig. 11 shows also that dc conductivity (σ_{dc}) increases with increasing Cu doping fraction. In particular, the trend of the total conductivity σ is generally related to the charge transport behavior of charge carriers. This trend has been widely noticed in conducting glasses [47], conducting polymers and doped crystalline solids [48].

4.5. Magnetic properties

The magnetic properties of MgO-doped Cu was studied by VSM measurements and performed at room temperature. The relation between the magnetization and the applied magnetic field is shown in Fig. 12a–d. It is clear from this figure the ferromagnetic behavior for all samples of $Mg_{1-x}Cu_xO$ (x = 0.05, 0.1, 0.15 and 0.2). This type of magnetic behavior may be explained on the basis of bound magnetic polarons (BMP) model suggested by Coey et al. [49]. Oxygen vacancies can induce a ferromagnetic coupling with Cu^{2+} ions through an indirect exchange. Similar results have been reported with Mn-, Co- and Ni-doped ZnO [50–52] and boost the results of the increase in the defect states with Cu^{2+} doping which leads to enhancing magnetic properties of $Mg_{1-x}Cu_xO$. Moreover, several reports have tried to explain the origin of ferromagnetism in MgO. It was believed that the ferromagnetic behavior is related to Mg vacancies and/or oxygen vacancies and lattice distortion in the MgO structure [53–66].

Table 3 shows the values of saturation magnetization, coercivity and the retentivity. It is clear that the values of the saturation magnetization and the retentivity found to decrease with the increase in Cu concentrations. Previously in TM-doped oxide systems, it has been reported that as the concentration of magnetic impurities is increased in the host oxide matrix, the saturation magnetic moment decreases which is attributed to the antiferromagnetic (AFM) interaction between the dopants [67]. Moreover, it is found that coercivity is improving with Cu concentration, i.e., increasing in coercivity with increasing Cu concentrations.

5. Conclusion

$Mg_{1-x}Cu_xO$ samples were successfully prepared by solid-state reaction. XRD results demonstrated samples with Cu content up to x = 0.15 like a single-phase solid solution of MgO rock salt structure type, while for x = 0.2, two phases were detected, namely MgO rock salt structure and Cu_2O cuprite cubic phase. The lattice constants increase with increasing the Cu content indicating that the Cu ion substitutes for the Mg ion in the MgO lattice. The crystallite size decreases with increasing the Cu concentration. The optical energy band was found to decrease with increasing the Cu content. The dielectric constant, the loss factor and the electrical conductivity increased with the doping concentration. The $Mg_{1-x}Cu_xO$ samples showed ferromagnetic

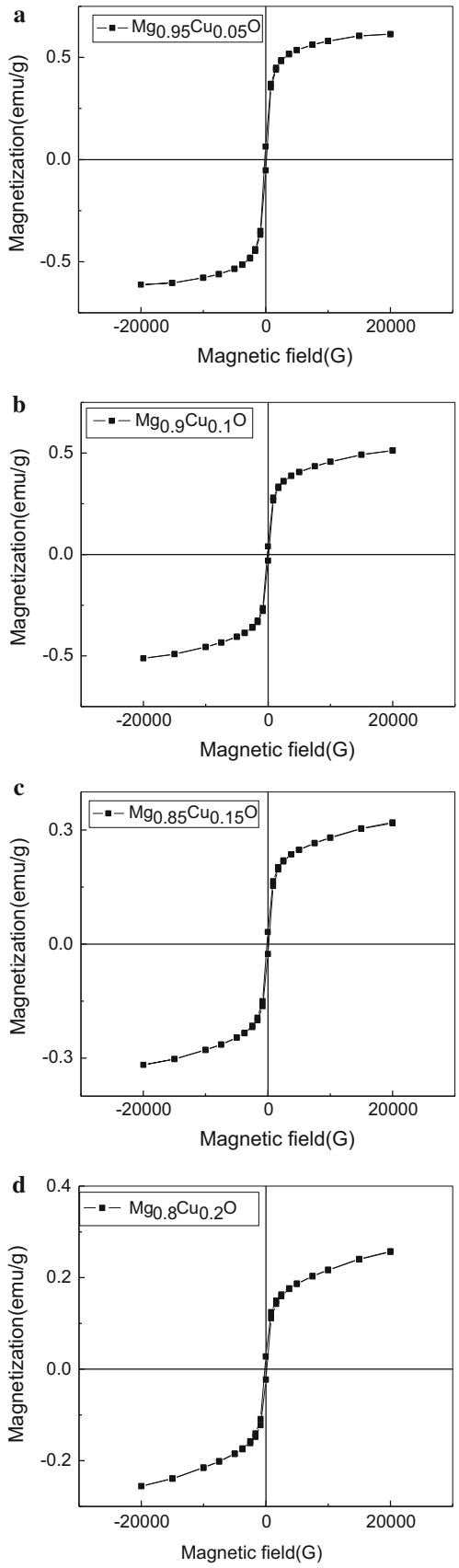

◀**Fig. 12** The magnetic hysteresis of $Mg_{1-x}Cu_xO$ samples at room temperature

Table 3 Values of magnetization M_s, coercivity H_c and retentivity M_r of $Mg_{1-x}Cu_xO$

Composition	M_s (emu/g)	H_c (G)	M_r (memu/g)
0.05	0.61329	98.032	57.946
0.1	0.51263	118.02	35.393
0.15	0.31891	133.2	28.828
0.2	0.25662	154.54	25.125

behavior. The saturation magnetization and the retentivity decrease with the increase in Cu concentrations. The coercivity increases with increasing Cu concentrations.

References

[1] G Spoto, E N Gribov, G Ricchiardi et al. *Prog. Surf. Sci.* **76** 71 (2004)
[2] K Kaviyarasu and P A Devarajan *Der Pharma Chem.* **3** 248 (2011)
[3] S Suresh and D Arivuoli *Dig. J. Nanomater. Biostruct.* **6** 1597 (2011)
[4] F Gu, S F Wang, M K Lü et al. *J. Cryst. Growth* **260** 507 (2004)
[5] B Nagappa and G T Chandrappa *Microporous Mesoporous Mater.* **106** 212 (2007)
[6] S M Maliyekkal, K R Antony and T Pradeep *Sci. Total Environ.* **408** 2273 (2010)
[7] K V Rao and C S Sunandana *J. Mater. Sci.* **43** 146 (2008)
[8] V R Orante-Barrn, L C Oliveira, J B Kelly et al. *J. Lumin.* **131** 1058 (2011).
[9] I EAgranovski, A YIlyushechkin, I S Altman, T E Bostrom and M Choi *Physica C* **1** (434) 115 (2006)
[10] T Mathews, R Subasri and O M Sreedharan *Solid State Ionics* **148** 135 (2002)
[11] N C Selvam, R T Kumar, L J Kennedy and J J Vijaya *J. Alloys Compd.* **509** 9809 (2011)
[12] L C Oliveira, E D Milliken and E G Yukihara *J. Lumin.* **133** 211 (2013)
[13] K D Bhatte, D N Sawant, K M Deshmukh and B M Bhanage *Particuology* **1** 384 (2012)
[14] R Kumar, A Subramania, N T K Sundaram, G V Kumar and I Baskaran *J. Membr. Sci.* **300** 104 (2007)
[15] F Granados-Correa, J Bonifacio-Mart´ınez, V H Lara, P Bosch and S Bulbulian *Appl. Surf. Sci.* **254** 4688 (2008)
[16] J M Hanlon, L Bravo Diaz, G Balducci, B A Stobbs, M Bielewski et al. *Cryst. Eng. Commun*. **17** 5672 (2015)
[17] M R Bindhu, M Umadevi, M Kavin Micheal, M VArasu and N Abdullah Al-Dhabi *Mater. Lett*. **166** 19 (2016)
[18] K Krishnamoorthy, G Manivannan, S J Kim, K Jeyasubramanian and M Premanathan *J. Nanopart. Res*. **14** (2012)
[19] R Darvishi Cheshmeh Soltani, M Safari and M Mashayekhi *Ultrason* **30** 123 (2016)

[20] N Salehifar, Z Zarghami and M Ramezani *Mater. Lett*. **167** 226 (2016)
[21] Patent: Jr E Carnall and S E Hatch, Magnesium oxide infrared transmitting optical elements, *US 3236595* **A** (1966)
[22] D C Harris *Infrared Phys. Technol.* **39** 185 (1998)
[23] T Misawa, Y Moriyoshi, Y Yajima, S Takenouchi and T Ikegami *Ceram. J. Ceram. Soc. Jpn.* **107** 343 (1999)
[24] L M Chen, X M Sun, Y N Liu and Y D Li *Appl. Catal. A. Gen.* **265** 123 (2004)
[25] M Jafarbegloo, A Tarlani, A Wahid Mesbah, J Muzart and S Sahebdelfar *Catal. Lett.* **146** 238 (2016)
[26] R Zanganeh, M Rezaei and A Zamaniyan *Adv. Powder Technol.* **3** 1111 (2014)
[27] E Florez, P Fuentealba and F Mondragón *Surf. Catal. Today* **133** 216 (2008)
[28] Y X Li and K J Klabunde *Langmuir* **7**1 388 (1991)
[29] V Štengl, S Bakardjieva, M Mǎríková, P Bezdička and J Šubrt *Mater. Lett.* **57** 3998 (2003)
[30] M B Gawande, P S Branco, K Parghi et al. *Catal. Sci. Technol.* **1** 1653 (2011)
[31] H Cui, X Wu, Y Chen, J Zhang and R I Boughton *Mater. Res. Bull*. **61** 511 (2015)
[32] F G Kuang, X Y Kuang, S Y Kang, Z H Wang and A J Mao *Chem. Phys. Lett.* **621** 52 (2015)
[33] P Thomson, D E Cox and J M Hasting *J. Appl. Cryst*. **20** 79 (1987)
[34] L Li, X Lin, G Li and H Inomata *J. Mater. Res*. **16** 3207 (2001)
[35] F Urbach *Phys. Rev*. **92** 1324 (1953)
[36] P D Fochs *Proc. Phys. Soc. B* **69** 70 (1956)
[37] J Liu, Y Lu, X Yang and X Yu *J. Alloys Compd.* **496** 261 (2010)
[38] A Asha Radhakrishnan and B Baskaran Beena *Indian J. Adv. Chem. Sci.* **2** 158 (2014)
[39] R Dalven *Phys. Rev. B* **8** 6033 (1973)
[40] W L Waren, G E Pike, K Vanheusden, D Domos and B A Tuttle *J. Appl. Phys.* **79** 9250 (1996)
[41] M L Hassan, S M Fadel, A A Ward, C M Moorefield and G R Newkome *Polym. Compos.* **37** 2734 (2016)
[42] S A Gad, A M Moustafa and A A Ward *J. Inorg. Organomet. Polym*. **25** 1077 (2015)
[43] H P De Oliveira, M VB dos Santos, C G dos Santos and C P de Melo, *Mater. Charact*. **50** 223 (2003)
[44] A F Ali, M L Hassan, A A Ward and E M El-Giar *Polym. Compos.* **38** 893 (2017)
[45] K A Mauritz *Macromolecules* **22** 4483 (1989)
[46] D K Pradhan, R N P Choudhary and B K Samantaray *Int. J. Electochem. Sci*. **3** 597 (2008)
[47] B Deb, S Bhattacharya and A Gosh *Europhys. Lett.* **3** 37005 (2011)
[48] A M Khalil, Mohammad L Hassan and A A Ward *Carbohydr. Polym.* **157** 503 (2017)
[49] J M D Coey, M Venkatesan and C B Fitzgerald *Nat. Mater.* **4173** (2005)
[50] Y M Sun Ph.D. Thesis (University of Science and Technology of China) (2000)
[51] U Koch, A Fojtik and H Henglein *Chem. Phys. Lett.* **122** 507 (1985)
[52] L Spanhel and M A Anderson *J. Am. Chem. Soc*. **113** 2826 (1991)
[53] J G Zhu and C Park *Mater. Today* **9** 36 (2006)
[54] L Guodong, J Shulin, Y Liangliang, F Guangtao and Y Changhui *J. Phys. Condens. Matter* **22** 046002 (2010)
[55] C Martínez-Boubeta, J I Beltrán, L Balcells, Z Konstantinović, S Valencia, D Schmitz et al. *Phys. Rev. B* **82** 024405 (2010)
[56] C M Araujo, M Kapilashrami, X Jun, O D Jayakumar, S Nagar et al. *Appl. Phys. Lett.* **96** 232505 (2010)
[57] J Li, Y Jiang, Y Li, D Yang, Y Xu and M Yan *Appl. Phys. Lett.* **102** 072406 (2013)
[58] F Wang, Z Pang, L Lin, S Fang, Y Dai and S Han *Phys. Rev. B* **80** (2009)
[59] T Uchino and T Yoko *Phys. Rev. B* **85** 012407 (2012)
[60] A Droghetti, C D Pemmaraju and S Sanvito *Phys. Rev. B* **81** (2010)
[61] N Kumar, D Sanyal and A Sundaresan *Chem. Phys. Lett*. **477** 360 (2009)
[62] S Xie, X Han, Q Kuang, Y Zhao, Z Xie and L Zheng *J. Mater. Chem.* **21** 7263 (2011)
[63] L Balcells, J I Beltrán, C Martínez-Boubeta, Z Konstantinović, J Arbiol and B Martínez *Appl. Phys. Lett*. **97** 252503 (2010)
[64] G Feng, S Van Dijken, J F Feng, J M D Coey, T Leo and D J Smith *J. Appl. Phys*. **105** 033916 (2009)
[65] K Mizunuma, M Yamanouchi, H Sato, S Ikeda, S Kanai et al. *Appl. Phys. Express* **6** 063002 (2013)
[66] K Tamanoi, M Sato, M Oogane, Y Ando, T Tanaka et al. *J. Magn Magn. Mater.* **320** 2959 (2008)
[67] A Singhala, S N Acharya, A K Tyagia, P K Mannab and S M Yusuf *Mater. Sci. Eng. B* **153** (1–3) 47 (2008)